Batteries & Supercaps

Research Article
doi.org/10.1002/batt.202100367

Chemistry Europe
European Chemical Societies Publishing

www.batteries-supercaps.org

VIP *Very Important Paper*

Biomass Hyaluronic Acid to Construct High-Loading Electrode with Fast Na^+ Transport Structure for $Na_3V_2(PO_4)_3$ Sodium-Ion Batteries

Yuyao Zhang,[a, b] Xiaoying Zhu,[a, b] Dan Kai,[c] and Baoliang Chen*[a, b]

Sodium-ion batteries (SIBs) are considered a promising candidate in green energy storage due to their considerable abundance. The low mass loading (less than 2.0 mg cm^{-2}) of SIBs-based cathodes cannot meet the energy density on the practical device level, which is mainly restricted by sluggish Na^+ transport. To the end, a facile and compatible strategy was demonstrated by utilizing hyaluronic acid (HA) binder to achieve fast ion transport and targeted energy density for $Na_3V_2(PO_4)_3$ (NVP) cathodes. As a novel functional aqueous binder, HA allowed cathodic materials to organize the unique conductive network. The network-like electrode structure could buffer volume changes during sodiation/desodiation process and provide bi-continuous charge transport channels for both Na^+ and electrons at the interface. HA promoted the formation of the stable solid permeable interface films, protecting the electrochemical stability of the cathode and ensuring its good cycle performance. These functions of HA binder enabled that NVP delivered a reversible discharge capacity of 107.3 mAh g^{-1} at 0.5 C (1 C = 117 mA g^{-1}), which showed no sacrifice of electrochemical performances with mass loading increasing from 1.1 to 4.4 mg cm^{-2}. Even at a high rate of 20 C, NVP-HA (loading 4.0 mg cm^{-2}) could reserve a good capacity of 76.8 mAh g^{-1} with the retention of 99.3% after 2000 cycles. This study provides a novel strategy to achieve high energy density for SIBs in large-scale energy storage.

Introduction

Sodium-ion batteries (SIBs) are expected to be a promising choice for lithium-ion batteries in the green energy storage due to its considerable abundance, and low cost of raw materials, as well as their similar electrochemical principle to lithium-ion batteries.[1] However, high powerful SIBs suffer from low mass loading, insufficient cycling lifespan and inferior rate capability as a result of their sluggish charge transfer.[2] Particularly, the transport pathway of Na^+ and electrons proportionally grows up with mass loading increasing, leading to high inner resistance and unsatisfactory energy density in practical applications.[3] So far, the mass loading of cathodes in the previous literature has been mostly less than 2.0 mg cm^{-2}.[4] Hence, numerous strategies have been studied to ameliorate the charge transport pathway at high mass loading, including interface modification and framework optimization via graphene, carbon nanotubes and so on.[5] However, these complicated strategies made an effort to solve this problem with intensive energy and cost. Moreover, excess packing of conductive carbon additives in the batteries would weaken binder adhesion and decrease the energy density.

Although tremendous studies aimed at developing and promoting the charge transfer of cathodic active materials, binders, as an indispensable part of cathode, were invariably ignored. Recent studies indicated that even a small dose of binders played a critical role in the electrochemical performance of SIBs.[6] Excellent binders were able to effectively organize the electrode structure with ideal features: i) The sturdy framework to hinder volume change and avoid collector separation;[7] ii) the optimization of conductive framework and the protection for electrodes to improve electrochemical performance.[8] An electrode structure with such ideal features might make it possible for high-performance SIBs at a high-mass loading.[9]

The traditional binder polyvinylidene difluoride (PVDF) suffers from weak inter-molecular forces, sluggish ion conductivity and toxic solvent processes.[10] In contrast, aqueous binders, such as sodium carboxymethyl cellulose (CMC) and konjac glucomannan,[11] have received increasing attention due to their efficient enhancement in electrochemical performances of cathode materials. Aqueous binders could effectively protect the electrode integrity and boost Na^+ transport via the formation of Na^+ coordinated bonding. For example, $Na_{0.44}MnO_2$ cathode delivered a stable lifespan of 800 cycles at 121 mA g^{-1} using CMC as binders instead of PVDF.[12] Polydopamine-$LiFePO_4$ cathode shows better capacity retention of 93% after 580 cycles over that of a PVDF-$LiFePO_4$ cell.[13] Therefore, the utilization of proper aqueous binder is accessible to optimize electrode structure to achieve high mass loading SIBs.

[a] *Y. Zhang, Prof. X. Zhu, Prof. B. Chen*
Department of Environmental Science
Zhejiang University
310058 Hangzhou, Zhejiang, China
E-mail: blchen@zju.edu.cn
[b] *Y. Zhang, Prof. X. Zhu, Prof. B. Chen*
Zhejiang Provincial Key Laboratory of Organic Pollution Process and Control
310058 Hangzhou, Zhejiang, China
[c] *Prof. D. Kai*
Institute of Materials Research & Engineering
*A*STAR (Agency for Science, Technology and Research)*
2 Fusionopolis Way, Innovis #08-03, 138634 Singapore

Supporting information for this article is available on the WWW under https://doi.org/10.1002/batt.202100367

Research Article
doi.org/10.1002/batt.202100367
Chemistry Europe
European Chemical Societies Publishing

However, many open challenges are still unsolved, which are related to the structure-performance mechanisms of aqueous binders in the enhancement of cathodes. Therefore, exploring the feasibility of binders in optimizing high-mass-loading electrodes was urgently needed for the development of advanced SIBs.

In this study, we demonstrated a green polysaccharide, hyaluronic acid (HA), as a novel aqueous binder to construct high-efficiency electrochemical performance at a high mass loading for cathodic electrodes. $Na_3V_2(PO_4)_3$ (NVP) was selected as a representative cathode due to its excellent performance in SIBs.[14] The excellent flexibility and adhesion strength of HA allowed it to be used in soft hydrogels, lubricants and cosmetic fillers,[15] which were beneficial characteristics for the performances of NVP cathodes at high mass loading. The experimental results indicated that HA constructed a porous conductive architecture to buffer volume changes and boost charge transfer at the solid interface. In addition, stable solid permeable interfaces (SPI) formed by HA enhanced the electrochemical stability of NVP cathodes. Due to the network-like architecture and stable SPI films, the NVP cathode (with a high mass loading of 4.4 mg) displayed a reversible rate capacity of 107.3 mAh g^{-1} at a current density of 0.5 C (1 C = 117 mA g^{-1}) and had a long lifespan of 2000 cycles at 20 C with a capacity retention of 99.3%. Our studies shed light on a scalable and cost-effective route that utilization of aqueous HA binder improved the performances of SIBs-based cathodes at high mass loading.

Results and Discussion

Structures and chemical properties of cathode

The morphology of as-prepared NVP powder was investigated by SEM and TEM. As shown in Figure S1(a and b), the NVP powder consisted of micrometric rhombohedral particles of 1–3 μm length. The structural characteristic and carbon content of NVP were measured by XRD and TGA. As shown in Figure S2(a), the diffraction peaks were consistent with that of rhombohedral $Na_3V_2(PO_4)_3$ (JCPDS. #62-0345). The carbon content of NVP was relatively low, which was ~4% as shown in Figure S2(b). After fabricating NVP, black carbon and binder into cathodes, the architecture of electrodes was confirmed by TEM. And the particle size of NVP in the electrodes became smaller than that of the freshly prepared NVP powder (Figure S1) due to the pulverization and grinding steps. The electrode using HA as a binder (denoted as NVP-HA) was observed to form a network-like structure. As shown in Figure 1(a), the network between black carbon and NVP was uniform and porous, which allowed bi-continuous channels for both transport of Na^+ and electron. In contrast, the electrode using CMC as a binder (denoted as NVP-CMC) glued small NVP particles tightly and formed the dense bulk-like structure of several micron widths, which would hinder the diffusion of Na^+. The dense architecture of the NVP-CMC electrode could be caused by the excessive bonding ability of the CMC binder. As shown in Figure 2(a and b), CMC possessed more ether and carboxyl functional groups than HA, leading that the tensile adhesion to separate Al foil pieces which were glued by CMC

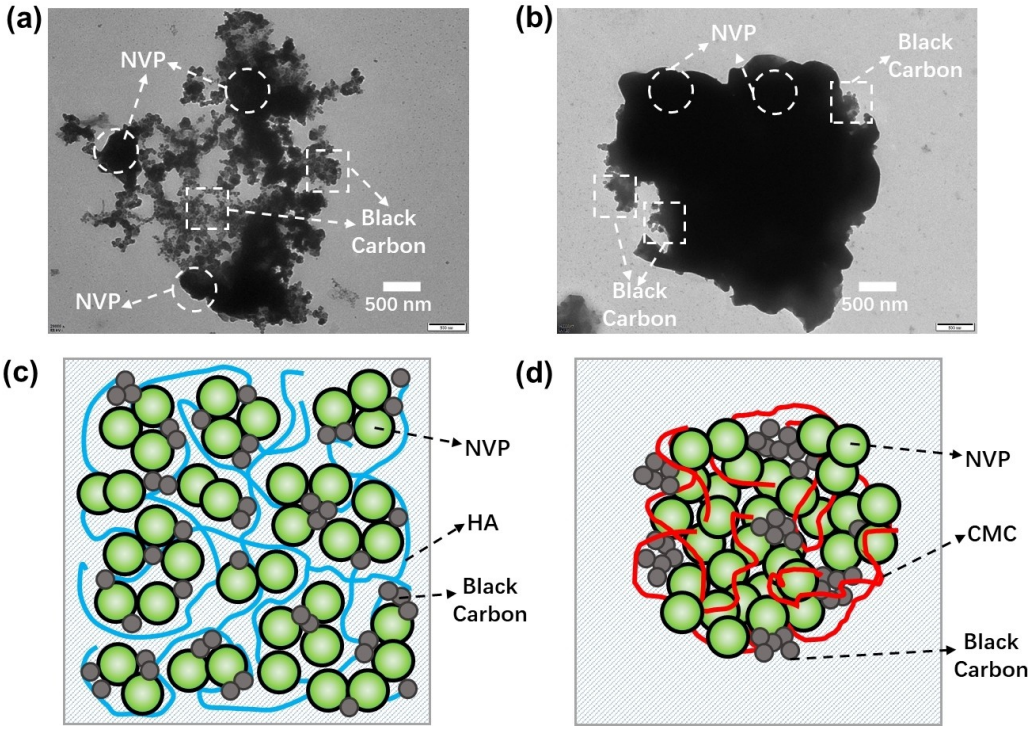

Figure 1. TEM of the structure in a) NVP-HA electrode and b) NVP-CMC electrode. Graphical illustration of the structure in c) the NVP-HA electrode and d) the NVP-CMC electrode.

Research Article
doi.org/10.1002/batt.202100367
Chemistry Europe
European Chemical Societies Publishing

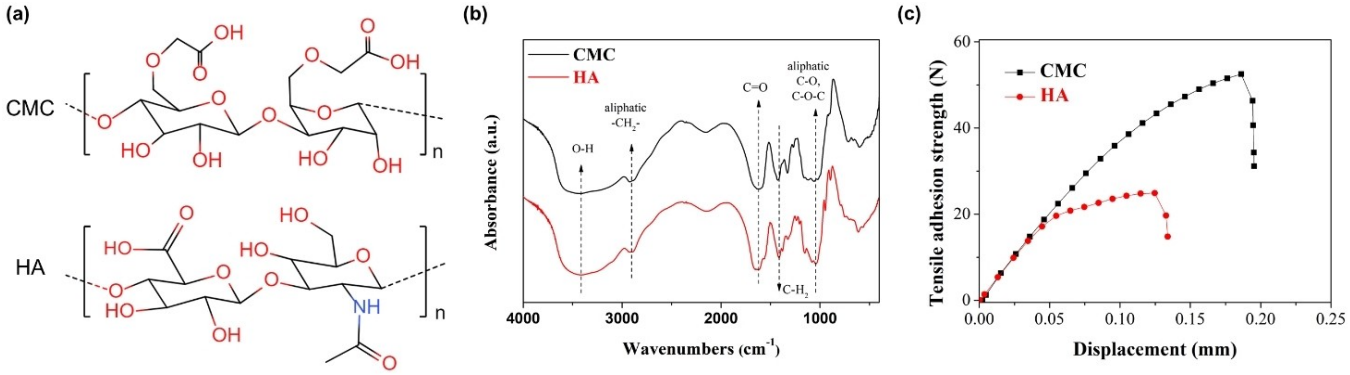

Figure 2. a) The molecular formula of CMC and HA. b) FTIR spectra of CMC and HA. c) The tensile adhesion-displacement curves of NVP-CMC and NVP-HA (contact area: 10 mm × 20 mm).

was stronger than that of HA.[11b] As shown in Figure 2(c), the CMC binder displayed an adhesion force of 52.5 N in the electrode, much higher than that of the HA binder (24.9 N). This excessive bonding ability of the CMC binder caused damage to the microstructure of the electrode instead, leading to the agglomeration of active materials and the sluggish diffusion of Na^+. Moreover, the tensile adhesion strength of HA was still larger than PVDF (13.8 N) and konjac glucomannan (19.7 N) in our previous work,[11a] meaning that HA was sturdy enough to bond the black carbon and NVP powder.

Electrochemical performance at high mass loading

High mass loading is an essential parameter for cathodes in practical applications. Up to now, the mass loading of NVP cathodes reported in the literature is mostly less than 2.0 mg cm^{-2}. Herein, the rate capability of the NVP-HA electrode with a high mass loading of 3.9–5.0 mg cm^{-2} was tested by cycling at 0.5–20 C in the sodium half battery system. Figure 3(a) compared the galvanostatic charge-discharge capacity profiles at 0.5 C of NVP-HA and NVP-CMC electrodes. There was a stable charge-discharge platform in the voltage range of 3.3–3.4 V, corresponding to the equilibrium electrode potential of V^{4+}/V^{3+} vs. Na^+/Na.[16] The minor splitting of the discharge plateau might be caused by the introduction of impurity ions during the NVP synthesis process. It was observed that NVP-HA had an initial discharge capacity of 107.3 mAh g^{-1} with a Coulombic efficiency of 99.1%, which was close to the theoretical capacity (117 mAh g^{-1}) of NVP. In the contrast, NVP-CMC possessed a lower discharge capacity of 97.5 mAh g^{-1}. Figures 3(b) and S3 showed that the types of binders could affect the rate capacity of electrodes. When the current density increased to 20 C, the NVP-CMC electrode exhibited a severe capacity loss with a discharge capacity of 45.0% (average for ten cycles). However, NVP-HA still delivered a high capacity of 66.6 mAh g^{-1}. The difference in the rate capability could be attributed to the diffusion rate of Na^+.[17] The dense bulk-like structure of the NVP-CMC electrode led to the sluggish transport of Na^+ and the concentration polarization, which could decrease the discharge capacity at high current density. The mass loading of NVP-HA increased from 1.1 to 4.4 mg cm^{-2}, the specific capacity showed little sacrifice at all rate stages (Figure 3b). It was attributed to the bi-continuous charge transport channels and fast Na^+ ions diffusion enhanced by HA binders, as discussed in the following part. When the mass loading of NVP-HA further increased to 10.5 mg cm^{-2}, the rate capability delivered an obvious drop due to the increasing inner resistance of charge transfer.

As shown in Figure 3(c), the cycling tests of electrodes at 0.5 C showed that NVP-HA could reserve a reversible capacity of 97.8 mAh g^{-1} with 91% capacity retention after 300 cycles, much better than the NVP-CMC (reserving 79.8 mAh g^{-1} with 85.5% capacity retention after 300 cycles). Specifically, the HA binder could effectively improve the cycling performance of NVP cathodes at a high current density. As shown in Figure 3(d and e), NVP-HA could retain a reversible capacity of 87.2 mAh g^{-1} after 1000 cycles at the current density of 5 C and could reserve 76.8 mAh g^{-1} after 2000 cycles at 20 C. In contrast, the capacity of NVP-CMC decreased to 67.8 mAh g^{-1} after 1000 cycles at 5 C and decreased to 34.0 mAh g^{-1} after 2000 cycles at 20 C. In contrast to the reported studies, NVP-HA was one of the best NVP cathodes with excellent cycling and rate performance at high mass loading (Table S1). The difference in cycling performance between two electrodes at high current density could also be attributed to the effect of binders on the micro-structure. Since HA binder could promote the cathode to weave a uniform network for bi-continuous charge transport channels as shown in Figure 1(c), it could achieve fast Na^+ insertion/extraction and avoid the non-equilibrium of concentration polarization even at an extremely high current density. This suggested that compared to traditional aqueous CMC binder, HA binder could promote the applications of NVP in high-power and high-energy-density scenarios. It also confirmed that the binder could effectively optimize the performance of the sodium-ion batteries although binders took only a tiny proportion in the whole cathodes.

Research Article
doi.org/10.1002/batt.202100367
Chemistry Europe
European Chemical Societies Publishing

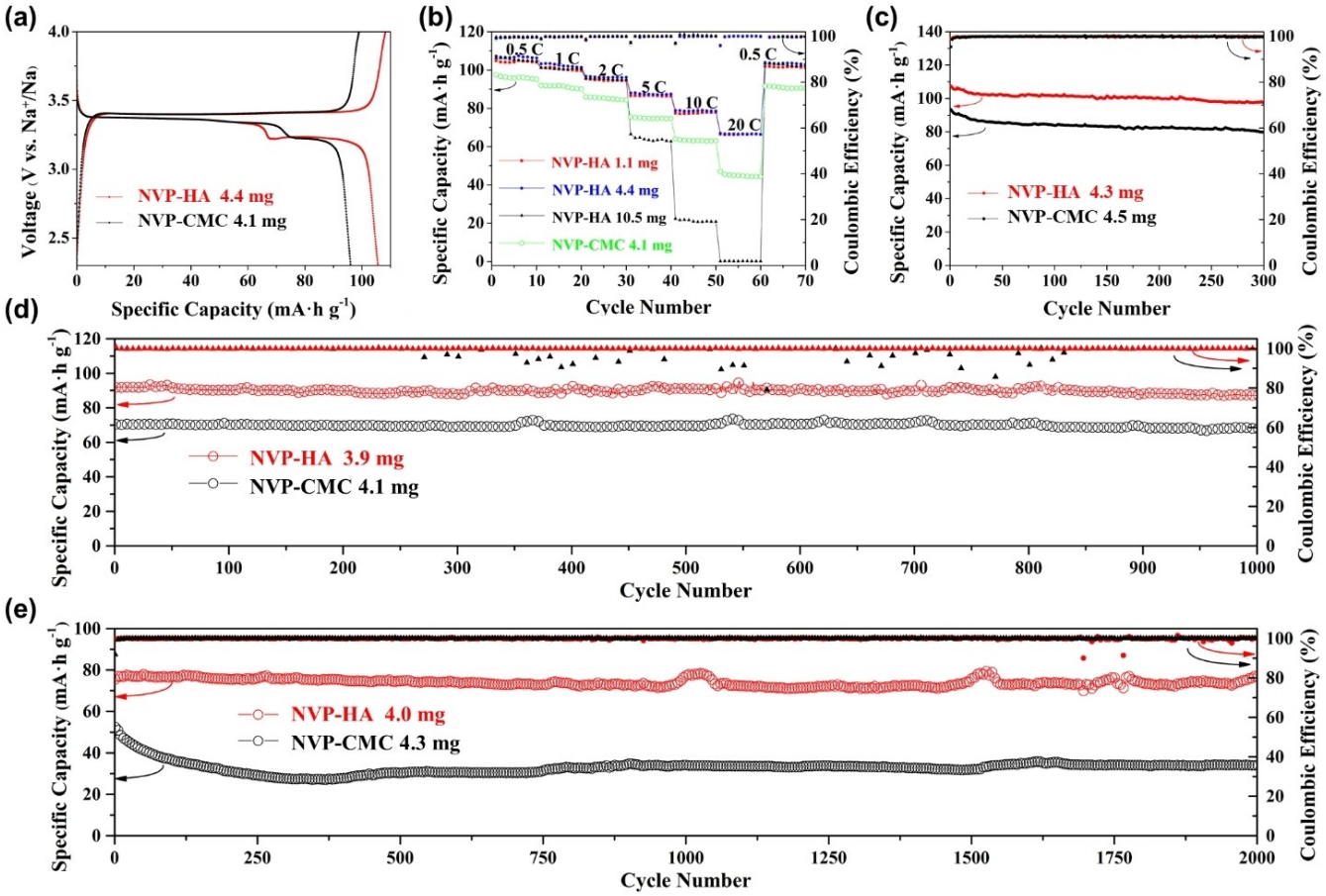

Figure 3. Rate capability and cycling performance of the electrodes using different binders. a) The galvanostatic charge-discharge capacity profiles at the 0.5 C current density and b) rate capability test at the current density of 0.5–20 C in different mass loading. Cycling performance at c) 0.5 C, d) 5 C and e) 20 C.

Fast Na^+ transport

The intrinsic structure, functional groups, mechanical properties, and electrochemical stability of binders play a critical role in the enhanced mechanism on the electrochemical performance of SIBs.[18] Here we found that the porous and uniform micro-structure of NVP-HA electrodes could promote the transport of Na^+ and further improve its charge-discharge performances. In this part, electrochemical measurements were performed to detect the kinetics of Na^+ diffusion in the sodium-ion batteries, including cyclic voltammetry analysis and electrochemical impedance spectra. As shown in Figure 4, the Nyquist plots of the sodium half batteries were measured at different temperatures. The interfacial charge-transfer resistance (denoted as R_{ct}) could be calculated via fitting the Nyquist plots (the equivalent circuit schematic was inserted in Figure 4a).[19] The diameter of the semicircle in the Nyquist plots represented the value of the interfacial resistance. Comparing Figure 4(a) and (b), the R_{ct} of NVP-HA sodium half batteries was much smaller than that of NVP-CMC at room temperature, indicating that HA binder could effectively reduce the interfacial resistances of Na^+ in the electrodes at the room temperature. Based on the relationship between the exchange current and temperature, we calculated the activation energy (E_a) of charge transfer via the Butler-Volmer equation [see Equation (1) in the Supporting Information] and Arrhenius equation [see Equation (2) in the Supporting Information).[11b] As a result, the calculated E_a was shown in the inset of Figure 4. The E_a of the exchange current for NVP-HA and NVP-CMC was 48.2 and 60.3 kJ mol^{-1}, respectively. The smaller E_a value of NVP-HA sodium half batteries confirmed that using HA as the binder for NVP could promote faster Na^+ transport and help reduce lower interfacial charge-discharge resistance. In contrast to PVDF (E_a: 78.5 kJ mol^{-1}) and konjac glucomannan (E_a: 64.4 kJ mol^{-1}),[11a] the ultra-low E_a of HA allowed NVP cathodes to deliver excellent performances even at a high mass loading.

In addition, we utilized cyclic voltammetry analysis to compare the Na^+ ions diffusion coefficient of the electrodes. The CV curves were recorded at the various sweep rate from 0.1–3.0 mV s^{-1} as shown in Figure 5(a and b). There was a pair of well-defined peaks in the charge-discharge processes, which suggested both NVP-HA and NVP-CMC had superb charge-discharge reversibility. Several theories were adopted to calculate the exact Na^+ diffusion coefficient in the previous reports.[20] Randles-Sevcik equation [see Equation (4) in the Supporting Information] was utilized to calculate the Na^+ diffusion coefficient based on the peak current value at the various sweep rates.[21] The slope of peak current *versus* the

Research Article
doi.org/10.1002/batt.202100367
Chemistry Europe
European Chemical Societies Publishing

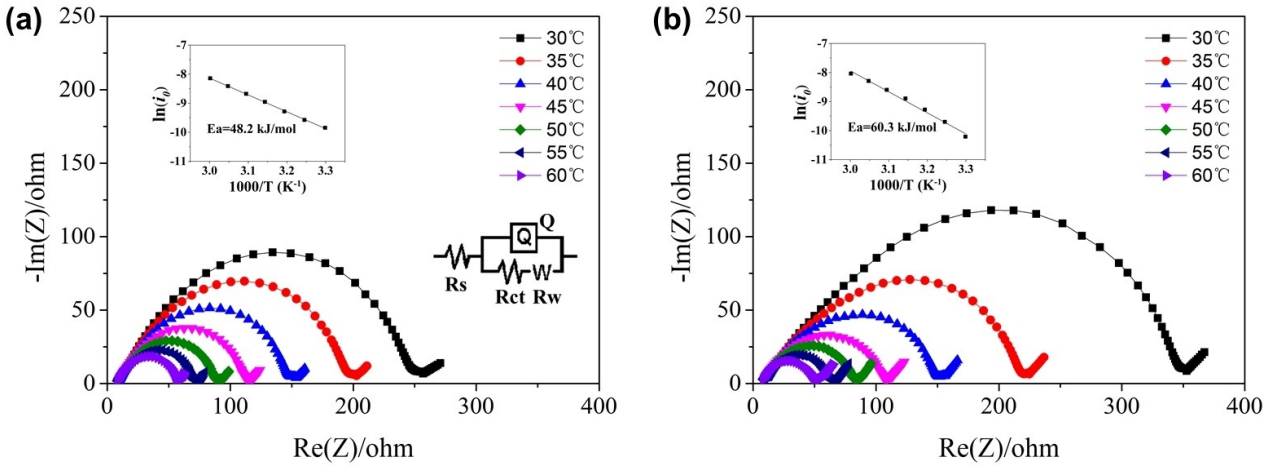

Figure 4. The electrochemical impedance spectra and the calculated activation energy of the exchange current for a) NVP-HA and b) NVP-CMC sodium half batteries.

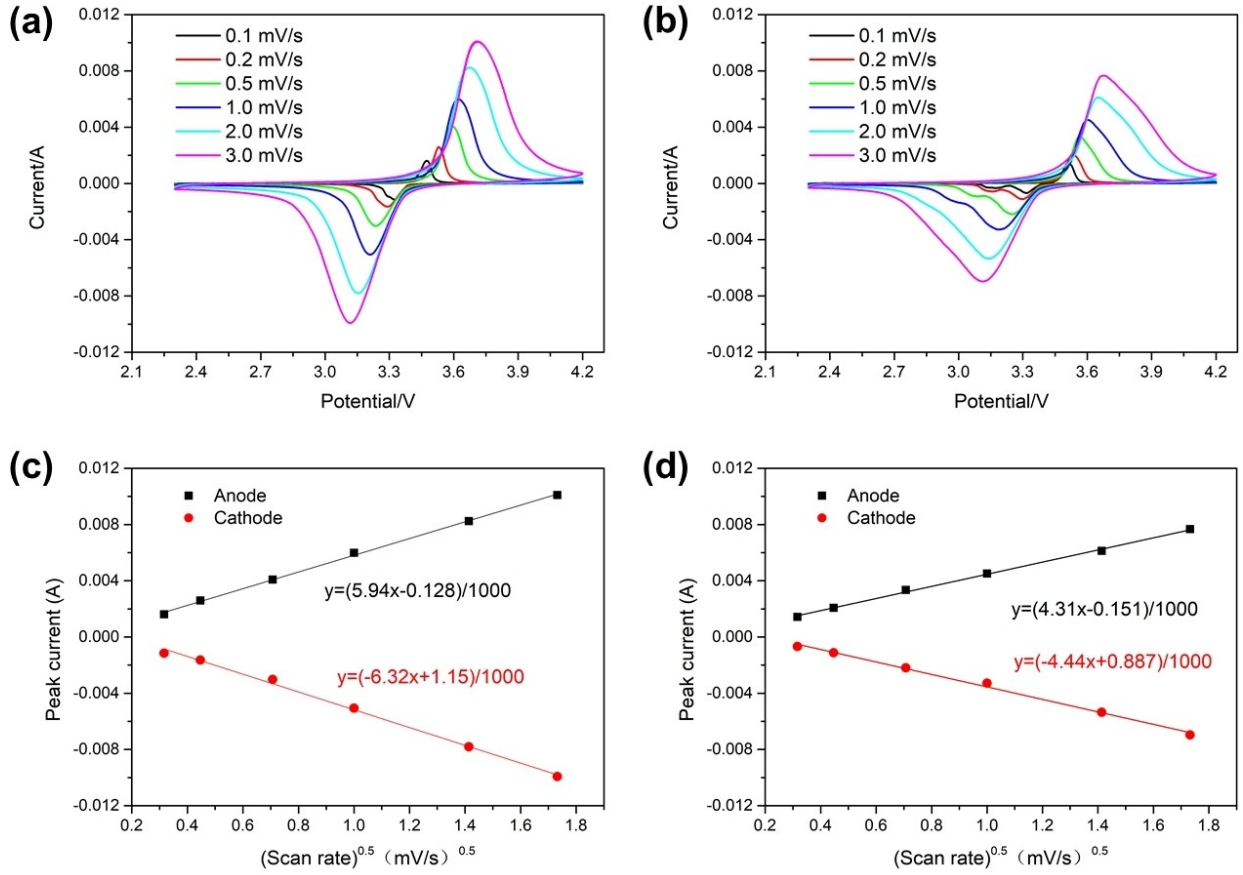

Figure 5. Cyclic voltammetry analysis of NVP-HA (a) and NVP-CMC (b) at the sweep rate range of 0.1–3.0 mV s^{-1}. Linear fitting of peak currents *versus* the square root of the sweep rate for the NVP-HA (c) and NVP-CMC (d).

square root of sweep rates was positively related to the coefficient of Na^+ diffusion as shown in Figure 5c and 5d. The calculated Na^+ diffusion was given in Table S2. It showed that the Na^+ diffusion of the NVP-HA electrode was larger than that of the NVP-CMC electrode whether it is based on the anodic peak current or the cathodic peak current. These results confirmed that HA binder could optimize the micro-structures of electrodes to enhance Na^+ ions diffusion.

Protection of SPI films

A solid permeable interface is usually defined as a cathode/electrolyte interface layer because of oxidation of the electrolyte, which can heavily influence the long cycling stability of cathodes.[22] It was reported that the uniform passivation layers from SPI films could effectively deactivate the functional groups and suppress the decomposition of electrolytes.[23] In our work, stable SPI films were also verified at the cathode interface, which could protect the integrity of the electrodes and improve the cycling performances. X-ray photoelectron spectra of C1s at the electrode interfaces were measured to analyze the SPI films. As shown in Figure 6, the C1s of both the fresh assembly NVP-HA and NVP-CMC electrodes peaked at around 284.6, 286.0 and 288.0 eV, corresponding to C–C, –CH_2– and –CO_2–, indicating the functional groups of their interfacial composites were similar as a polysaccharide.[24] However, a difference appeared between the two electrodes after 300 cycles at 0.5 C. There was a new C1s peak at 290.0 eV in the NVP-HA that experienced 300 charge-discharge cycles, corresponding to RO-CO_2-Na or other degraded composites of electrolytes.[25] These degraded composites at the electrode interface were able to construct SPI films to protect the chemical structure of the cathodes. Moreover, the protection from SPI films could keep stable electrochemical performances for long-term cycles, and ameliorate the kinetics at the interface between electrode and electrolyte.[26] On the contrary, the C1s spectra of NVP-CMC delivered a relatively weak peak at 290.6 eV after 300 cycles in Figure 6(b), suggesting that there were no shaped films like RO-CO_2-Na composites covering on the cathode interface. It was inferred that the uniform and porous micro-structures of NVP-HA could favor the deposition of SPI films.

To confirm the protective ability of SPI films to NVP cathodes, the electrochemical interfacial resistance of the sodium half batteries was measured after hundreds of cycles. The electrochemical impedance spectra of both electrodes were measured as shown in Figure 7. Before long-term charge-discharge cycles, the NVP-HA electrode had a smaller interfacial resistance than the NVP-CMC electrode. After hundreds of charge-discharge cycles, the interfacial resistance of NVP-HA gradually stabilized in the range of 243 to 171 Ω. Instead, the interfacial resistance of NVP-CMC increased from 400 to 586 Ω continuously. Given that XPS detected SPI films at the interface of the NVP-HA electrode, the improvements of interfacial resistance could be mainly attributed to the protection and passivation of SPI films. And the continuously increasing interfacial resistance of NVP-CMC could be caused by collapsing electrode structure without the protection of SPI films. In brief, our efforts revealed that non-active components of electrodes

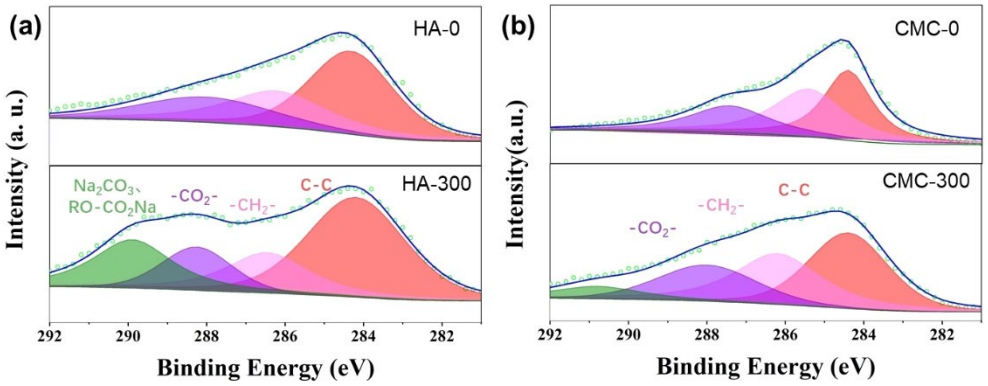

Figure 6. The XPS of a) NVP-HA and b) NVP-CMC before and after 300 charge-discharge cycles at the current density of 0.5 C.

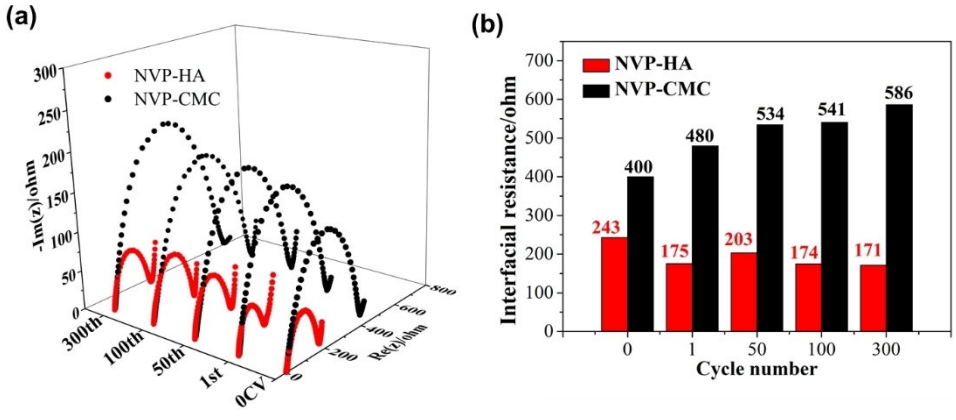

Figure 7. a) Nyquist spectra and b) interfacial resistance of NVP-HA and NVP-CMC after 0, 1, 50, 100 and 300 charge-discharge cycles.

Research Article
doi.org/10.1002/batt.202100367

could effectively ameliorate SPI films to improve the electrochemical performance of SIBs.

The SEM morphology of both electrodes after 300 cycles was observed to check the mechanical stability of binders. As shown in Figure 8(a), the NVP-HA electrode kept the initial morphology with an integral, uniform and porous structure. As for the structure of NVP-CMC, there were several cracks at the surfaces (Figure 8b). In addition, the active material of NVP-HA was well attached to Al foils at the cross-section of an electrode (Figure 8c). While using CMC as binders, there were ~20 μm cracks between the active material and Al foil. The cracks could severely impact the transport of electrons. Given that the CMC binder had a stronger tensile adhesion force than the HA binder (Figure 2c), it was interesting that NVP-CMC was more prone to cracking than NVP-HA. This contradiction was explained by the difference in electrode structures. As the CMC binder had powerful adhesion strength, it tended to a dense bulk for electrode structure. When the electrode experienced sodiation and desodiation processes, its volume would shrink and expand periodically. During such periodic volume fluctua-

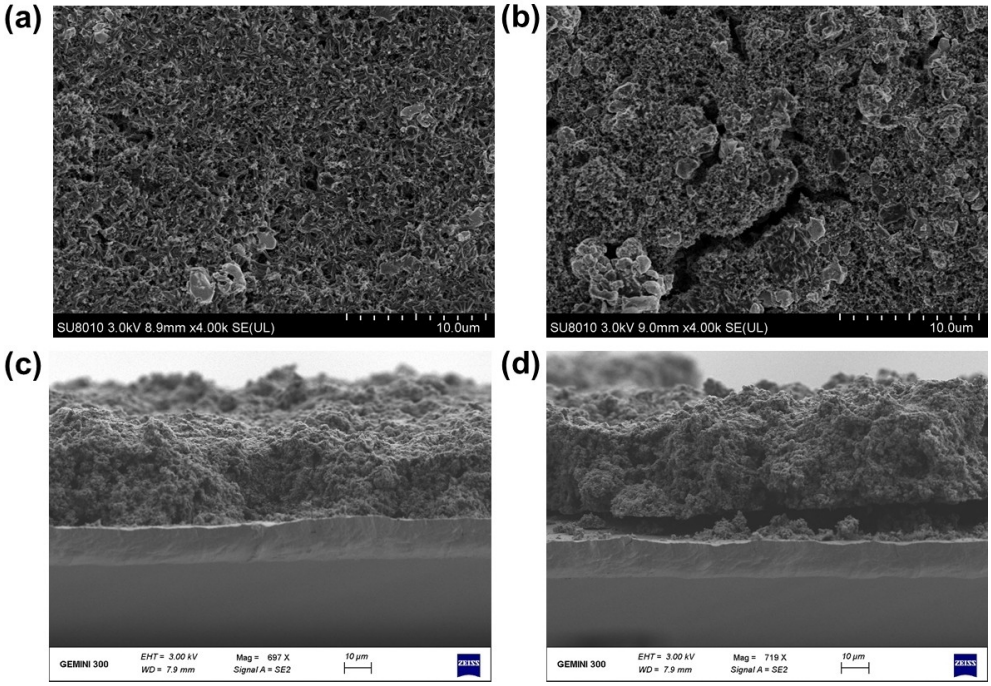

Figure 8. SEM morphology of a) NVP-HA and b) NVP-CMC after 300 cycles, and the corresponding cross-section SEM images of c) NVP-HA and d) NVP-CMC.

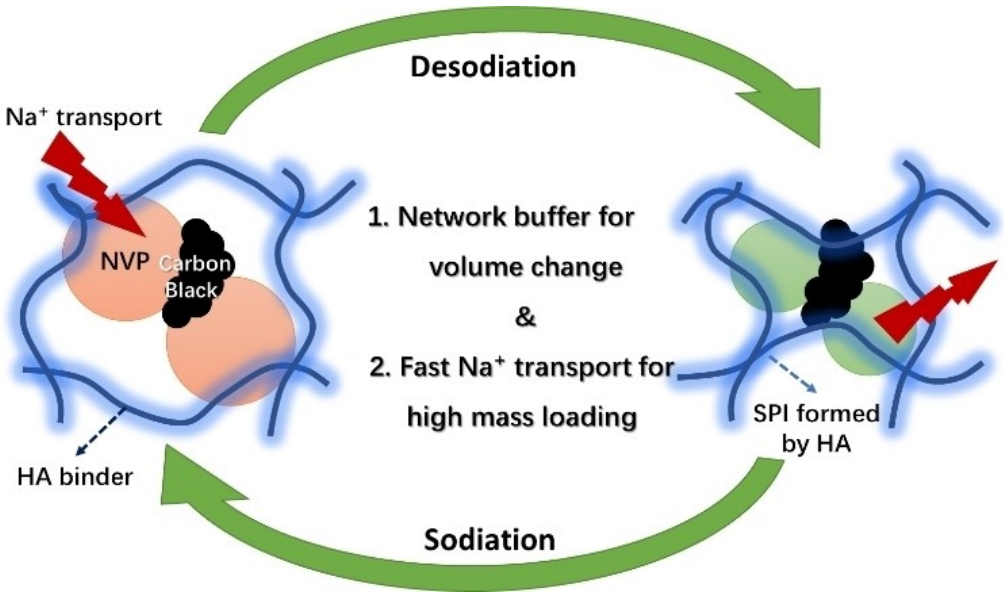

Figure 9. The schematic for dual functions of HA binder to achieve high electrochemical performance for NVP cathodes.

tions, the electrode with a too dense structure was fragile and was likely to cause cracks. Instead, the porous network-like structure of NVP-HA provided the buffer space for the volume breathing, leading to a more stable mechanical integrity of the electrode. Hence, SEM morphology evidenced that the network-like structure of NVP-HA could protect its mechanical integrity and ensure its good cycle performance.

In brief, the functions of hyaluronic acid binder to achieve high electrochemical performance for the NVP cathodes are summarized in Figure 9. At the molecular level, the difference in functional groups between two binders is the main reason for their effect on the electrochemical performance. Excess carboxyl groups in CMC lead to a dense bulk of NVP, which hinder the Na^+ transfer and is prone to cracking during sodiation/desodiation processes. Instead, the proper ratio of hydroxyl and carboxyl groups provides a network bonding structure that can resist the volume breathing of cathodes. Further, this network-like structure builds a bi-continuous channel to enhance the transport of electrons and Na^+ and delivers enough surface area to form stable SPI films. These advantages can effectively protect the structure of the electrode and extend the service life of SIBs.

Conclusion

In conclusion, our efforts demonstrated that HA could be used as a functional aqueous binder that could achieve long-life and high-rate performance for high-mass loading NVP cathodes. Compared to traditional aqueous CMC binder, HA binder had weaker adhesion strength but provided bi-continuous charge channels and stable SPI films. This structural advantage led to stable mechanical integrity and fast charge transfer. Therefore, the NVP-HA cathode delivered a reversible discharge capacity of 107.3 mAh g^{-1} at the current density of 0.5 C, which showed no sacrifice of electrochemical performances with mass loading increasing from 1.1 to 4.4 mg cm^{-2}. Even at a high rate of 20 C, NVP-HA (mass loading 4.0 mg cm^{-2}) could still reserve a good capacity of 76.8 mAh g^{-1} with the retention of 99.3% after 2000 cycles. Our efforts provide a facile and promising strategy to allow electrodes with high energy density for advanced SIBs.

Experimental Section

Chemicals and materials

Sodium hydroxide (≥96.0% purity), ammonium dihydrogen phosphate (≥99.5% purity), hydrochloric acid (36.0%–38.0%), sodium metal (≥99.5% purity) and sodium carboxymethyl cellulose (chemically pure) were purchased from Sinopharm Chemical Reagent Co., Ltd. Ammonium metavanadate (99% purity) was purchased from Aladdin Bio-Chem Technology Co., Ltd. Hyaluronic was purchased from Freda Biopharm, China. Citric acid monohydrate (99.0%–102.0% purity), black carbon (Super P Conductive, 99 +%, metals basis) was purchased from Alfa Aesar Chemical Co., Ltd. Glass microfiber filters (GF/D) were purchased as separators from Whatman Co., Ltd. Liquid electrolyte (1.0 mol L^{-1} $NaClO_4$ in the mixture of diethyl carbonate and ethylene carbonate (DEC: EC, 1:1 vol%), with 5% fluoroethylene carbonate (FEC)) was purchased from DoDoChem Co., Ltd.

Synthesis of NVP

NVP was synthesized via the sol-gel method reported in our previous works.[11a] Firstly, 3 mmol $NH_4H_2PO_4$ and 3 mmol NaOH were dissolved in 20 mL deionized water at room temperature. Then, 2 mmol NH_4VO_3 powder was added to the solution. The mixture was stirred and heated to approximately 85 °C to form a transparent solution. Then, 2 mmol citric acid monohydrate was slowly added into the solution at the temperature of 85 °C. Subsequently, the solution evaporated into a dry gel at 85 °C for 2 h. The gel was ground into powder as the precursor for NVP. At last, the precursor was heated at 350 °C for 5 h and then heated at 800 °C for 12 h under a high-purity N_2 atmosphere. It is worth noting that the air-tightness of the tube furnace is crucial for the synthesis of NVP to avoid O_2 oxidizing NVP.

Material characterization

Thermogravimetric analysis (TGA) was applied to analyze the carbon contents of NVP with Mettler Toledo STARe System TGA2. X-ray diffraction (XRD) was used to characterize the crystal structure of NVP with Cu K_α radiation over a 2θ range of 5°–90° (Bruker D8 Advance). The surface morphologies and cross-section of cathodes were imaged by scanning electron microscopy (Hitachi SU-8010 and ZEISS GeminiSEM 300, respectively). The microscale structures of cathodes were detected by transmission electron microscopy (TEM) with Tecnai G2 F20 S-TWIN. Fourier transform infrared spectroscopy (FTIR) characterized the functional groups of HA and CMC with a wave number of 4000–400 cm^{-1} (Nicolet 6700, America). Universal testing machine determined the tensile adhesion strength of HA and CMC with Zwick/Reoll Z020. Cathode materials were glued between two aluminum collectors by binders with a contact area of 10 mm × 20 mm. The machine fixes one end and stretches the other end at the speed of 0.1 mm min^{-1}, as demonstrated in Figure S4 (Supporting Information). The surface chemical structures of cathodes were analyzed by X-ray photoelectron spectra (XPS), which was performed with Al K_α 1486.6 eV using a Thermo Scientific ESCALAB 250Xi.

Electrochemical measurements

Coin-type cell 2032 was assembled for electrochemical measurements. The cathode slurry was composed of NVP: black carbon: binder (1.0% HA or 1.0% CMC in water) at a mass ratio of 8:1:1. The slurry mixtures were crushed and ground thoroughly via a mortar and pestle, and then was coated on a circular Al-based current collector (diameter: 15 mm) to manufacture the cathode. Each cathode contained a high loading mass of NVP at 3.9–5.0 mg cm^{-2}. The current collector coated with slurry was dried in a vacuum oven at 105 °C. Sodium metal was utilized as the anode in the 2032 coin-type cells. 1.0 mol L^{-1} $NaClO_4$ solution (EC: DEC 1:1 vol%, 5% FEC) was utilized as electrolyte liquid. Coin-type cell 2032 was assembled at an Ar atmosphere in a glove box ($O_2 \leq$ 0.01 ppm, $H_2O \leq 0.01$ ppm). Electrochemical impedance spectra (EIS) of cells were determined at a frequency of 0.1–10^5 Hz in a CHI760E electrochemical station system (Chenhua Instruments, China). Cyclic voltammetry curves were tested at the rate of 0.1–3.0 mV s^{-1} in the CHI760E station. Galvanostatic charge-discharge of cells was tested using a voltage of 2.3–4.0 V in a Neware Battery Testing System. Electrochemical performances of cycling stability and rate capability were determined at the current density of 0.5–20 C.

Appendix A. Supplementary Data

A survey of electrochemical properties of NVP cathodes (Table S1), calculated Na^+ ions diffusion coefficient (Table S2), SEM image and TEM image of NVP (Figure S1), X-ray diffraction and thermogravimetric curve of NVP (Figure S2), discharge profiles at different current densities (Figure S3), schematic diagram of tensile adhesion strength tests (Figure S4).

Author Contributions

Y. Y. Z. conceptualized the material design, performed the experiments, and drafted the manuscript. X. Y. Z. and D. K. analyzed the data and revised the manuscript. B. L. C. supervised the project and guided at all stages.

Acknowledgements

*This project was supported by the National Natural Science Foundation of China (Grant 22136004 and 21621005), and the National Key Technology Research and Development Program of China (Grant 2018YFC1800705). The authors gratefully acknowledge the financial support from the Agency of Science, Technology and Research (A*STAR).*

Conflict of Interest

The authors declare no conflict of interest.

Data Availability Statement

Data sharing is not applicable to this article as no new data were created or analyzed in this study.

Keywords: binder · high mass loading · hyaluronic acid · $Na_3V_2(PO_4)_3$ · sodium-ion batteries

[1] a) H. J. Huang, R. Xu, Y. Z. Feng, S. F. Zeng, Y. Jiang, H. J. Wang, W. Luo, Y. Yu, *Adv. Mater.* **2020**, *32*, 1904320; b) Z. Z. Zhang, Y. C. Du, Q. C. Wang, J. Y. Xu, Y. N. Zhou, J. C. Bao, J. Shen, X. S. Zhou, *Angew. Chem. Int. Ed.* **2020**, *59*, 17504–17510; *Angew. Chem.* **2020**, *132*, 17657–17663.
[2] a) W. Duan, Z. Zhu, H. Li, Z. Hu, K. Zhang, F. Cheng, J. Chen, *J. Mater. Chem. A* **2014**, *2*, 8668–8675; b) J.-Z. Guo, P.-F. Wang, X.-L. Wu, X.-H. Zhang, Q. Yan, H. Chen, J.-P. Zhang, Y.-G. Guo, *Adv. Mater.* **2017**, *29*, 1701968; c) Y. Xu, Q. Wei, C. Xu, Q. Li, Q. An, P. Zhang, J. Sheng, L. Zhou, L. Mai, *Adv. Energy Mater.* **2016**, *6*, 1600389.
[3] a) Y. He, P. Bai, S. Gao, Y. Xu, *ACS Appl. Mater. Interfaces* **2018**, *10*, 41380–41388; b) Z. Lv, M. Yue, M. Ling, H. Zhang, J. Yan, Q. Zheng, X. Li, *Adv. Energy Mater.* **2021**, *11*, 2003725.
[4] a) Y. Cai, F. Liu, Z. Luo, G. Fang, J. Zhou, A. Pan, S. Liang, *Energy Storage Mater.* **2018**, *13*, 168–174; b) S. Li, J. Guo, Z. Ye, X. Zhao, S. Wu, J.-X. Mi, C.-Z. Wang, Z. Gong, M. J. McDonald, Z. Zhu, K.-M. Ho, Y. Yang, *ACS Appl. Mater. Interfaces* **2016**, *8*, 17233–17238.
[5] a) X. Cao, A. Pan, B. Yin, G. Fang, Y. Wang, X. Kong, T. Zhu, J. Zhou, G. Cao, S. Liang, *Nano Energy* **2019**, *60*, 312–323; b) H. Chen, B. Zhang, X. Wang, P. Dong, H. Tong, J.-C. Zheng, W. Yu, J. Zhang, *ACS Appl. Mater. Interfaces* **2018**, *10*, 3590–3595; c) X. Rui, W. Sun, C. Wu, Y. Yu, Q. Yan, *Adv. Mater.* **2015**, *27*, 6670–6676.
[6] a) Y. Su, X. Feng, R. Zheng, Y. Lv, Z. Wang, Y. Zhao, L. Shi, S. Yuan, *ACS Nano* **2021**, *15*, 14570–14579; b) H. A. Lee, M. Shin, J. Kim, J. W. Choi, H. Lee, *Adv. Mater.* **2021**, *33*, 2007460; c) H. W. Zhang, Z. S. Lv, Q. H. Liang, H. R. Xia, Z. Q. Zhu, W. Zhang, X. Ge, P. Yuan, Q. Y. Yan, X. D. Chen, *Batteries & Supercaps* **2020**, *3*, 101–107.
[7] a) Y. Yoda, K. Kubota, H. Isozumi, T. Horiba, S. Komaba, *ACS Appl. Mater. Interfaces* **2018**, *10*, 10986–10997; b) S. Guo, H. Li, Y. Li, Y. Han, K. Chen, G. Xu, Y. Zhu, X. Hu, *Adv. Energy Mater.* **2018**, *8*, 1800434.
[8] a) H. Gao, W. Zhou, J.-H. Jang, J. B. Goodenough, *Adv. Energy Mater.* **2016**, *6*, 1502130; b) J. Jeon, J.-K. Yoo, S. Yim, K. Jeon, G. H. Lee, J. H. Yun, D. K. Kim, Y. S. Jung, *ACS Sustainable Chem. Eng.* **2019**, *7*, 17580–17586.
[9] a) D. L. Guo, J. W. Qin, Z. G. Yin, J. M. Bai, Y. K. Sun, M. H. Cao, *Nano Energy* **2018**, *45*, 136–147; b) D. T. Ma, Y. L. Li, J. B. Yang, H. W. Mi, S. Luo, L. B. Deng, C. Y. Yan, P. X. Zhang, Z. Q. Lin, X. Z. Ren, J. Q. Li, H. Zhang, *Nano Energy* **2018**, *43*, 317–325.
[10] J. Zhao, X. Yang, Y. Zhang, X. J. Loh, X. Hu, G. Chen, F. Du, Q. Yan, *J. Mater. Chem. A* **2019**, *7*, 1548–1555.
[11] a) Y. Zhang, X. Zhu, D. Kai, Y. Jiang, Q. Yan, B. Chen, *J. Mater. Chem. A* **2021**, *9*, 9864–9874; b) J. Zhao, X. Yang, Y. Yao, Y. Gao, Y. Sui, B. Zou, H. Ehrenberg, G. Chen, F. Du, *Adv. Sci.* **2018**, *5*, 1700768.
[12] V. Dall'Asta, D. Buchholz, L. G. Chagas, X. Dou, C. Ferrara, E. Quartarone, C. Tealdi, S. Passerini, *ACS Appl. Mater. Interfaces* **2017**, *9*, 34891–34899.
[13] T. Sun, Z.-J. Li, H.-G. Wang, D. Bao, F.-L. Meng, X.-B. Zhang, *Angew. Chem. Int. Ed.* **2016**, *55*, 10662–10666; *Angew. Chem.* **2016**, *128*, 10820–10824.
[14] a) D. X. Wang, N. Chen, M. L. Li, C. Z. Wang, H. Ehrenberg, X. F. Bie, Y. J. Wei, G. Chen, F. Du, *J. Mater. Chem. A* **2015**, *3*, 8636–8642; b) X. H. Zhang, X. H. Rui, D. Chen, H. T. Tan, D. Yang, S. M. Huang, Y. Yu, *Nanoscale* **2019**, *11*, 2556–2576; c) W. Li, Z. Yao, Y. Zhong, C.-a. Zhou, X. Wang, X. Xia, D. Xie, J. Wu, C. Gu, J. Tu, *J. Mater. Chem. A* **2019**, *7*, 10231–10238.
[15] a) H. Lee, S. M. Dellatore, W. M. Miller, P. B. Messersmith, *Science* **2007**, *318*, 426–430; b) T. J. Taylor, S. S. Stivala, *J. Polym. Sci. Part B* **2003**, *41*, 1263–1272.
[16] Y. J. Fang, L. F. Xiao, X. P. Ai, Y. L. Cao, H. X. Yang, *Adv. Mater.* **2015**, *27*, 5895–5900.
[17] Q. Zheng, H. M. Yi, X. F. Li, H. M. Zhang, *J. Energy Chem.* **2018**, *27*, 1597–1617.
[18] L. Ling, Y. Bai, Z. Wang, Q. Ni, G. Chen, Z. Zhou, C. Wu, *ACS Appl. Mater. Interfaces* **2018**, *10*, 5560–5568.
[19] R. Klee, M. J. Aragon, P. Lavela, R. Alcantara, J. L. Tirado, *ACS Appl. Mater. Interfaces* **2016**, *8*, 23151–23159.
[20] a) J. Liu, Y. Liu, Y. Wang, C. Wang, Y. Xia, *Batteries & Supercaps* **2019**, *2*, 867–873; b) W. Li, Z. Yao, C.-a. Zhou, X. Wang, X. Xia, C. Cu, J. Tu, *Small* **2019**, *15*, 1902432; c) Y. Li, J. Qian, M. Zhang, S. Wang, Z. Wang, M. Li, Y. Bai, Q. An, H. Xu, F. Wu, L. Mai, C. Wu, *Adv. Mater.* **2020**, *32*, 2005802.
[21] H. Kim, J. Lee, H. Ahn, O. Kim, M. J. Park, *Nat. Commun.* **2015**, *6*, 7278.
[22] a) H. Yu, Y. Gao, X. Liang, *J. Electrochem. Soc.* **2019**, *166*, A2021–A2027; b) S. Malmgren, K. Ciosek, M. Hahlin, T. Gustafsson, M. Gorgoi, H. Rensmo, K. Edstrom, *Electrochim. Acta* **2013**, *97*, 23–32.
[23] M. Zhang, Y. Li, F. Wu, Z. Wang, Y. Bai, C. Wu, *J. Mater. Chem. A* **2021**, *9*, 10780–10788.
[24] R. Liu, Y. Xu, B. Chen, *Environ. Sci. Technol.* **2018**, *52*, 7043–7053.
[25] a) Y. Tang, J. Deng, W. Li, O. I. Malyi, Y. Zhang, X. Zhou, S. Pan, J. Wei, Y. Cai, Z. Chen, X. Chen, *Adv. Mater.* **2017**, *29*, 1701828; b) A. M. Haregewoin, A. S. Wotango, B.-J. Hwang, *Energy Environ. Sci.* **2016**, *9*, 1955–1988.
[26] S. J. Rezvani, R. Parmar, F. Maroni, F. Nobili, A. Di Cicco, R. Gunnella, *J. Phys. Chem. C* **2020**, *124*, 26670–26677.

Manuscript received: November 27, 2021
Revised manuscript received: December 21, 2021
Accepted manuscript online: December 30, 2021
Version of record online: January 28, 2022